Dyes and Pigments 95 (2012) 587–599

Contents lists available at SciVerse ScienceDirect

Dyes and Pigments

journal homepage: www.elsevier.com/locate/dyepig

A novel barbituric acid-based azo dye and its derived polyamides: Synthesis, spectroscopic investigation and computational calculations

Mohammad Reza Zamanloo*, Amir nasser Shamkhali, Masoumeh Alizadeh, Yagoub Mansoori, Golamhassan Imanzadeh

Department of Applied Chemistry, Faculty of Basic Science, University of Mohaghegh Ardabili, Ardabil, Iran

ARTICLE INFO

Article history:
Received 6 November 2011
Received in revised form
6 May 2012
Accepted 14 May 2012
Available online 2 July 2012

Keywords:
Azo dye
Barbituric acid
Computational calculations
Tautomerism
Polyamides
UV–vis spectroscopy

ABSTRACT

5-[(3,5-dicarboxyphenyl)azo]-barbituric acid, an azo-based aromatic diacid was prepared and fully characterized by FT IR, ^{1}H and ^{13}C NMR along with UV–vis absorption spectroscopy. The effects of varying pH and solvent upon the absorption spectrum of the azo dye were investigated. The optimized molecular structures of possible tautomeric forms and HOMO–LUMO energies of expecting preferred forms of the synthesized heterocyclic azo dye have been calculated using density functional theory, (B3LYP) methods with TZVP basis set level and Polarizable Continuum Model (PCM) model for solvation effect. The calculations showed that the most probably preferred form of the azo dye in gas phase and solution was a hydrazone-keto form. FT IR and UV–vis spectroscopy, DSC, TGA and XRD techniques were used to obtain the characteristics and structural features of the monomer-synthesized polyamides. The influence of organic solvents on the absorption spectra of the polymers along with viscosity measurements (0.19–0.44 dl/g), solubility and film formability of the synthesized polyamides were also investigated.

1. Introduction

Azo dyes derived from heterocyclic systems exhibit modified dying and optical properties relative to the azo benzenoid compounds. The subject is clarified in higher sensitivity of their absorption spectroscopic properties to structural changes. Direct influence of heteroatomes on the molecular orbitals, low aromaticity and hyperpolarizibility along with dependence of energy levels to substituent groups are the most important characteristics of heterocyclic compounds to access the diversity of optical absorption properties. Bathochromic shift in the absorption spectra of hetarylazo dyes is the most important features of their optical properties [1–7]. Azo dyes derived from various heterocyclic coupling components such as thiazole, thiophene and pyrazole are the instances of desired materials [8–15]. On the other hand, the possibility of tautomerism in hetarylazo compounds which induce light fastness and moreover coordination ability to metal cations to forming complexes can verify their application fields. It is well known that azo dyes with heterocyclic components exhibit good tinctorial strength and brighter dyeing than those derived from benzenoids [16–19].

Azobarbituric acid derivatives are another class of hetarylazo compounds that characterize to show various tautomeric structures in their free acid form. They have versatile utilities as their salts, metal complexes, solid solutions, inclusion and intercalation compounds [20,21]. These organic pigments are distinguished by high tinctorial strength, great hiding power, very good light fastness properties, and excellent solvent fastness properties as well as heat resistance which all indebt to more tautomeric structures. Hence, they are applied as pigments in printing inks, distempers or emulsion paints. Some of the spectroscopic properties and tautomeric forms of azobarbituric acid derivatives have been described in recent publications [22–25].

Technical applications of azo-dye compounds mainly depend on the oxidative, thermal and solvent resistance, along with lightness strength and optical properties of the azo chromophore. More superior properties can be offered in the polymeric form in view of higher processability, free-standing film formability and photoactivity [26,27]. Three main procedures have developed to introduce an azo chromophore into a polymeric structure, including: blending of the organic molecular pigment with the polymeric matrix, chemical bonding of the pigment to the polymer structure and polymerizing the pigment-containing monomers resulted to

* Corresponding author. Tel.: +98 4515514702; fax: +98 4515514701.
E-mail addresses: zamanlou@yahoo.com, mrzamanloo@uma.ac.ir (M.R. Zamanloo).

0143-7208/$ – see front matter © 2012 Elsevier Ltd. All rights reserved.
http://dx.doi.org/10.1016/j.dyepig.2012.05.028

the polymers with the chromophore in side chains or in the main chain. Non-leaching behavior combined with uniform dispersion of colorants in polymer matrix without aggregation is the major advantage of the last method. Hence, the design and synthesis of functional colorants with polymerization ability have received considerable attention [28–35]. Polyamides, as the most applicable engineering plastics, are of great importance in this regard for their applications as self-coloured materials. Their usages as fiber form in man-made textiles take a special attention because of the requirement to stability and improved thermal properties especially at colored state [36–40].

According to our literature survey there are a few publications on barbituric acid-based azo dye polymers and their metal complexes. In this research, a new azo dye monomer was synthesized from barbituric acid and utilized to prepare a series of aromatic polyamides. The optimized molecular geometries of seven tautomeric forms of the synthesized hetarylazo monomer were calculated to distinguish the most stable configuration playing an important contribution in controlling spectroscopic properties. The monomer and polymers with the chromophore in side chains were evaluated for absorption spectroscopic aspects in aqueous and organic media using UV–vis measurements.

2. Experimental

2.1. Materials

The used chemicals were purchased from Merck Chemical Co., Fluka Chemical Co., and Aldrich Chemical Co. 5-aminoisophethalic acid was recrystallized from a mixture of N,N′-dimethylformamide (DMF)/water (3/1 V). 4,4′-diaminodiphenyl ether, 4,4′-diaminodiphenyl sulfone, 3,3′-diaminodiphenyl sulfone, 4,4′-diaminodiphenylmethane and 1,5-diaminonaphtalene were recrystallized from ethanol/water (3/1 V). 1,4-diphenylenediamine, 1,3-diphenylenediamine and 4-methyl-1,3-phenylenediamine were sublimed under reduced pressure. N,N′-dimethylacetamide (DMAC), N-methyl pyrrolidone (NMP) and pyridine were stirred over powdered calcium hydride or KOH overnight and then distilled under reduced pressure. Triphenylphosphite (TPP) was used without further purification. Anhydrous calcium chloride was dried under vacuum at 120 °C for 5 h.

2.2. Instruments and measurements

Melting points were determined on a Stuart SMP-3 melting point apparatus with a heating rate of 2 °C/min and not corrected. Fourier transform infrared (FT IR) spectra (in KBr pellets) were recorded on a perkin-Elmer RX-I spectrometer in the region of 4000–400 cm^{-1}. Vibration transition frequencies are reported in wave-number (cm^{-1}). Band intensities are assigned as weak (w), medium (m), shoulder (sh), strong (s) and broad (br). ^1H NMR and ^{13}C NMR spectra were recorded on a Bruker 300 MHz and 75 MHz spectrometer respectively, in DMSO–d_6 using tetramethylsilane (TMS) as an internal reference. Multiplicity of proton resonances was designated as singlet (s), broad (br) and multiplet (m). A double beam shimadzu UV-1650 PC spectrophotometer was used to record the absorption spectra over a wavelength range of 200–600 nm. Quartz cuvettes were used for measurements in solution. The diffuse reflectance spectra were recorded on powder samples with a Color GrapgTM spectrophotometer (Miton Roy Co). Differential Scanning Calorimetry (DSC) was done using an NETSCH DSC 200 F_3. The measurements were performed in the range of 25–400 °C at a heating rate of 10 °C/min under a nitrogen atmosphere as cycles consisting of 1st heating–cooling–2nd heating scans. Glass transition temperatures (*Tg*) were read at the middle of inflections in DSC traces. Thermogravimetric analysis (TGA) was performed with a PL 1500-TGA at a heating rate of 10 °C/min under nitrogen atmosphere. Inherent viscosities (η_{inh}) were obtained on 0.5% (w/v) polyamide solutions in H_2SO_4 at 30 °C by an Ostwald Routine Viscometer (Germany). Wide-angle x-ray diffraction (XRD) measurements were performed at room temperature on a Siemens D500 x-ray diffractometer (Germany) using Ni-filtered Co–Ka radiation.

2.3. Synthesis

2.3.1. 5-[(3,5-dicarboxyphenyl)azo]-barbituric acid (monomer) (**IV**)

5-aminoisophthalic acid (1.00 g, 5.52 mmol) was dissolved in 12.0 ml of a mixture of DMF and concentrated hydrochloric acid, (2/1 V). The solution was then cooled to −5–0 °C and sodium nitrite (0.427 g, 6.18 mmol, 14.2% aq) was added dropwise with vigorous stirring. The resultant mixture was stirred for 30 min at 0 °C, and then 0.707 g (5.52 mmol) of barbituric acid dissolved in 5 ml of aqueous solution of sodium acetate 5% (w/v) was added portionwise to the diazonium solution. The resulting mixture was stirred for 3.5 h at that temperature. A yellow solid product separated upon dilution with cold water which was filtered off and washed several times to reach neutral state. The crude dye was purified by reprecipitating of DMF solution to a large amount of water to afford a bright yellow powder (1.66 g, 94%, vacuum dried at 100 °C for 3 h). d.t. 319–326 °C, FT IR(KBr, cm^{-1}): 3450 (m), 3200 (m), 3079 (m), 2848 (w), 1720 (s), 1670 (s), 1643 (m), 1527 (s), 1458 (s), 1434 (s), 1397 (s), 1278 (s), 1218 (s), 1085 (w). ^1H NMR (DMSO–d_6, *δ*, ppm): 8.25 (s, 2H), 8.34 (m, 1H), 11.34 (s, 1H), 11.53 (s, br, 1H), 14.06 (s, br, 1H). ^{13}C NMR (DMSO–d_6, *δ*, ppm): 166.5 ($C_{11, 12}$), 162.1 (C_4), 160.2 (C_2), 150.2 (C_1), 142.9 ($C_{6, 10}$), 133.1 (C_8), 126.9 ($C_{7, 9}$), 121.7 (C_5), 119.4 (C_3). Elemental analysis calculated for $C_{12}H_8N_4O_7$: C, 45.00%; H 2.52%; N, 17.50%; Found: C, 44.12%; H, 3.20%; N, 16.95%.

2.3.2. Synthesis of model compound

In a 50 ml round-bottom flask equipped with a magnetic stirrer and reflux condenser, were placed 0.500 g (1.56 mmol) of dicarboxylic acid (**IV**), 0.335 g (3.12 mmol) of *p*-toluidine, 1.938 g (6.24 mmol, 1.64 ml) of TPP, 4.0 ml of DMAC, 0.8 ml of pyridine and 0.78 g of $CaCl_2$. The mixture was heated with stirring at 110 °C for 6 h under argon atmosphere. After cooling, 100 ml of methanol was poured into the resulting mixture and the yellowish precipitate was filtered off, washed thoroughly with methanol and dried in vacuum at 100 °C for 4 h. The purification of the product was performed by reprecipitating from DMF to methanol (0.51 g, 65.4%), d.t. 335–341 °C. FT IR (KBr, cm^{-1}): 3425 (s), 3133 (m), 3067 (m), 2920 (m), 2852 (m), 1741 (s), 1722 (s), 1665 (s), 1650 (s), 1597 (s), 1533 (s), 1518 (m), 1451 (w), 1420 (m) 1395 (s), 1317 (s), 1279 (m). ^1H NMR (DMSO–d_6, *δ*, ppm): 2.28 (s, 6H), 7.17 (d, $J = 7.2$ Hz, 4H), 7.67 (d, $J = 7.2$ Hz, 4H), 8.25 (m, 2H), 8.32 (s, 1H), 10.42 (*t*, $J = 14.8$ 2H), 10.88 (s, 1H), 11.39 (s, br, 1H), 14.23 (s, br, 1H). ^{13}C NMR (DMSO–d_6, *δ*, ppm): 165.3 (C_{11}), 164.7 (C_4), 150.2 (C_2), 142.3 (C_1), 137.2 ($C_{7, 9}$), 137.0 (C_{15}), 133.4 (C_{12}), 133.37 ($C_{6, 10}$), 129.5 ($C_{14, 16}$), 124.0 (C_5), 120.9 (C_8), 119.4 ($C_{13, 17}$), 118.8 (C_3), 21.0 (C_{18}) ppm.

2.3.3. Synthesis of polyamides (PAa-h)

The phosphorylation polycondensation method was used to prepare the polyamides. As a typical case: In a 50 ml round-bottom flask equipped with a magnetic stirrer and reflux condenser, were placed 0.500 g (1.56 mmol) of dicarboxylic acid (**IV**), 0.308 g (1.56 mmol) of 4,4′-diamino diphenyl methane, 1.938 g (6.2 mmol, 1.64 ml) of TPP, 5.0 ml of DMAC, 0.50 ml of pyridine and 0.780 g of $CaCl_2$. The reaction mixture was heated with stirring at 120 °C for 8 h under argon atmosphere. As the polycondensation proceeded, the solution gradually became viscous. After cooling, 100 ml of

Table 1
Calculated energies (E/hartree) of the azo and hydrazone tautomers of azo-dye (**IV**).

Tautomer	E/Hartree	Tautomer	E/Hartree
Azo-Keto (1)	−1207.7102694		
Azo-Enol (2)	−1207.7413862	Hydrazone-Keto (5)	−1207.7665129
Azo-Enol (3)	−1207.7101748	Hydrazone-Keto (6)	−1207.7313351
Azo-Enol (4)	−1207.6987158	Hydrazone-Keto (7)	−1207.7019972

methanol was poured into the resulting viscous mixture with rapid stirring and the yellow precipitate was filtered off, washed thoroughly with methanol and dried in vacuum at 100 °C for 4 h (0.352 g, 93.6%), d.t. > 350 °C. The inherent viscosity of the resulting polymer, PA**b**, was 0.42 dl/g (Conc. H_2SO_4, 30 °C).

2.3.4. Polymer film preparation

An approximately 8 wt% clear solution of each of the polymers in NMP, DMAC and DMF was transferred on a glass plate according to the drop coating method. The subject was placed at RT in a low humidity air chamber for 2 weeks to evaporate the solvent. The thin films were removed from the glass plate by immersing in water.

2.3.5. Geometry optimization of tautomeric forms of the azo dye

All of the tautomeric structures of the azo dye were considered for geometry optimization using Density Functional Theory (DFT) method by B3LYP hybrid functional at TZVP basis set level [41–43]. These DFT calculations were performed using Firefly Ab initio package [44,45]. Important bond lengths and angles for two probably preferred tautomeric structures (**2** and **5**) were given in Table 6. Since during the optimization calculations on azo-enol structure (**2**), the enolic hydrogen showed more tendency to join to N atom, the O–H bond length was held fixed. Polarizable Continuum Model (PCM) model was used to describe the solvent effect on tautomeric stabilization [46]. Moreover, in order to evaluate the UV–vis spectra, the HOMO and LUMO energies of the preferred tautomeric forms were also calculated.

3. Results and discussion

3.1. Structural identification and verification of monomer

The synthetic pathway of the monomer is shown in Scheme 1. The key step of the synthesis is in situ formation of the diazonium salt of 5-amino isophthalic acid. Limited solubility of the amine compound and sensitivity of the process to the reaction pH are parameters should be considered in reaction controlling. The first step is carried out in the combined solvent (DMF/H_2O) and the second one is take placed in the presence of sodium acetate.

Thin layer chromatography (TLC) and CHN analysis were used to confirm the purity of the monomer and FT IR, ^1H and ^{13}C NMR along with UV–vis spectroscopic techniques as well as quantum chemical calculations were used to evaluate the chemical structure and structural composition of the compound. It is well known that azo dyes having barbituric acid moieties as prepared in this study can exist in some tautomeric forms as shown in Scheme 2 for azo dye (**IV**) [22–25].

To have a better understanding and describe the experimental results DFT calculations have been performed for seven tautomers of compound **IV**. The optimized molecular structures including azo-enol and hydrazone-keto tautomers are depicted in Fig. 1.

Their calculated energies represented in Table 1 illustrate the hydrazone-keto tautomers are more stable than their azo-enol counterparts. This is in accordance with other literature data for similar compounds indicating a larger stability of hydrazone tautomers over azo forms [47,48].

On the other hand, two tautomeic structures (**5**) and (**2**) possess minimal energy between their partner tautomers. The relative energy difference and Gibbs free energies of these two comparable tautomeric forms are depicted in Table 2.

The tautomeric equilibrium constant, K_T, between azo and hydrazone tautomers can be calculated using the following equation [47]:

$$K_T = \exp - \Delta G/RT \quad (1)$$

where the gas constant R is 8.3145×10^{-3} kJ mol^{-1} K^{-1} and the temperature T is 298 K. The quantity ΔG is the difference between the Gibbs free energies of the given tautomers which is defined as $G_{Hydrazone(5)} - G_{Azo(2)}$. The mole fractions of individual tautomers are calculated using the following equations [49]:

$$N_{Azo} = 1/(1 + K_T), \quad N_{Hydrazone} = K_T/(1 + K_T) \quad (2)$$

giving more than 96% of hydrazone-Keto form at room temperature.

The relative energies of the tautomeric structures (**2**) and (**5**) were also calculated (PCM) in two polar protic and aprotic media (MeOH and DMSO) to evaluate the solvent effects on their stability

Table 2
Calculated relative energies (ΔE/kJ mol^{-1}), Gibbs free energies (G/Hartree[a]), tautomeric equilibrium constant (K_T) and mole fractions of the azo and hydrazone tautomeric forms (N_{Azo} and $N_{Hydrazone}$) of azo dye (**IV**) at 296 K.

$\Delta E_{Azo\ (2)}$/ (kJ mol^{-1})	$\Delta E_{Hydrazone\ (5)}$/ (kJ mol^{-1})	$G_{Azo\ (2)}$/ (Hartree)	$G_{Hydrazone\ (5)}$/ (Hartree)
65.970	00.000	−1207.581039	−1207.606986
ΔG/kJ mol^{-1}	K_T	$N_{Azo\ (2)}$	$N_{Hydrazone\ (5)}$
−67.860296	27.388	0.0352	0.9648

[a] 1 Hartree = 2625.50 kJ mol^{-1}.

Table 3
Selected interatomic distances and dihedral and torsion angles for the azo and hydrazone tautomeric forms (**2**) and (**5**) of the azo dye (**IV**) calculated at TZVP basis set level.

Selected bond distances (Å)		
	Azo (2)[a]	Hydrazone (5)
N18-N19	1.27	1.32
N19-C20	1.38	1.33
C20-C22	1.39	1.46
C22-O27	1.34	1.27
O27-H29	0.68	1.84
H29-N18	1.67	1.02
N18-C1	1.42	1.41
Selected angles (°)		
C20-N19-N18	116.90	121.63
C1-N18-N19	116.27	120.80
C20-C22-O27	123.10	123.00
C22-C20-N19-N18	0.00	0.08
C6-C1-N18-N19	0.00	0.20
C21-C20-N19-N18	180.00	179.96
C2-C1-N18-N19	179.98	179.81

[a] Calculations were performed on the fixed structure (**2**).

Table 4
Influence of solvent on the absorption properties of azo dye (**IV**).[a]

Solvent	$_{max}$ (nm)	ε_{max} (Lmol^{-1} cm^{-1})	$\rightarrow\pi^*$	ε_{max} (Lmol^{-1} cm^{-1})	$\rightarrow\pi_*$	ε_{max} (Lmol^{-1} cm^{-1})
DMAC	382	27,640	334	8260	270	10,180
DMSO	383	26,360	332	18,900	262	12,240
THF	376	18,170	328	6900	254	8960
HOAc	380	22,350	329	7020	250	16,320
MeOH	388	26,230	330	8680	260	15,320

[a] Measured at concentration of 5×10^{-5} M.

Table 5
Influence of different pH conditions on λ_{max} (nm) of the azo dye[a].

pH	λ_{max} (nm)	ε_{max} ($Lmol^{-1}$ cm^{-1})
3.0	380.0	80,140
5.0	380.0	95,120
7.0	384.0	83,290
9.0	380.0	75,340
11.0	368	84,360

[a] Measured at concentration of 10^{-5} M.

and absorption properties. As seem from Fig. 2, hydrazone tautomer shows solvation stability slightly more than azo form (0.8 kJ/mol), although this energy decrease is substantial for both structures in respect to gas phase. On the other hand, the deference of the relative energies has been greater in protic methanol compared with aprotic DMSO. Calculated dipole moment for two isomers (**2**) and (**5**) being 3.69 and 2.54 D respectively probably define the result.

Table 3 provides DFT results for selected interatomic distances and angles of the two tautomeric forms (**2**) and (**5**) based on the following structural labeling.

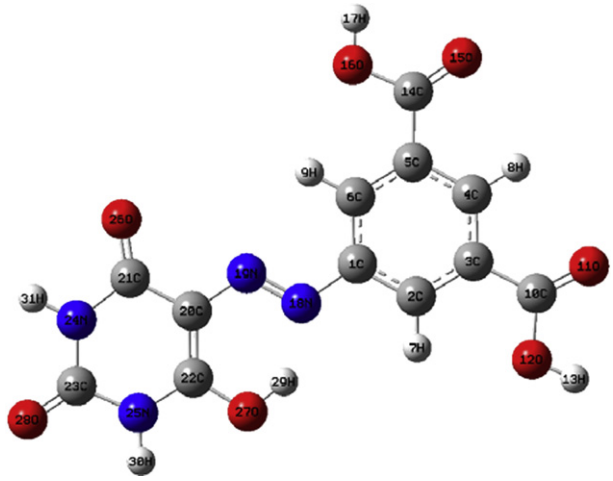

Structure (**2**) used for interatomic distance and angle calculations.

Both tautomers show planar geometry with torsion and dihedral angles of zero and 180° respectively between barbituric unit and the aromatic ring. Major variations in geometry are at bonds participating in azo–hydrazone tautomerism including azo bond N18–N19, hydrogen bonds at N19 and O27 atoms (N19–H29 and O27–H29) as well as N19–C20 and C22–O27 bonds. The remainder of the bonds and angles in both tautomers do not change significantly. On the other hand, bond distance N18–C1 in both azo and hydrazone forms is in the range of a single bond length, indicating no substantial resonance character between the chromophore and the aromatic ring being in contrast with prediction of the planar arrangement of both tautomers.

Table 6
Solubility of azo dye (**IV**).[a]

Solvent	H_2O	MeOH	THF	Acetone	HOAc	Py	DMF	DMSO	DMAc
Solubility	±	±	±	−	±	±	+	+	+

[a] 5% (w/v); +, Soluble at room temperature; ±, Partially soluble on heating; −, Insoluble.

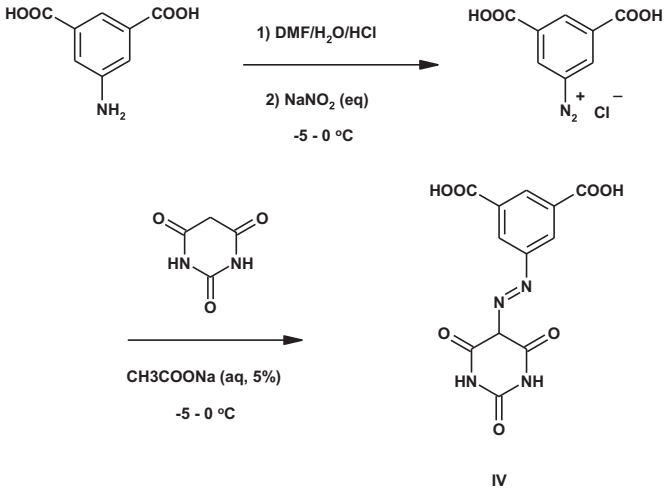

Scheme 1. The synthetic route of the monomer (compound **IV**).

In order to find some clues about the absorption spectra, the highest occupied molecular orbital (HOMO) as well as HOMO−1 and lowest unoccupied molecular orbital (LUMO) energy levels diagrams of two comparative tautomers are calculated both in gas phase and solution, Fig. 3. According to this schematic, the electronic transitions in hydrazone form (**5**) take place in slightly smaller wavelengths than the azo form. On the other hand, charge distribution in HOMO and LUMO diagrams of both tautomers are not considerably different which indicate electron transfer between the two components of the chromophore, namely hyperpolarizibility, should not perform during the electronic transition. In addition, since localization and distribution of the electron density of HOMO and LUMO on all of a system are measures of light fastness, the finding orbital diagrams propose a good photostability for azo dye (**IV**) [50,51]. Furthermore, the azo–hydrazone tautomerism may also improve light fastness due to reducing in electron density at azo group by intra-molecular resonance-assisted hydrogen bonding which results in lowered sensitivity towards photochemical oxidation [52,53].

According to the findings of quantum chemical calculations the synthesized azo dye should mostly exist in the hydrazone form (**5**) at room temperature both as a separated molecule or solvent-interacted. Since the investigated solvents were proton donor-acceptor types, solvation stability could indicate the stabilization effect of such interactions acting also in concentrated media like solid state.

UV–visible absorption spectra of the azo dye were recorded over the wavelength range of 200–800 nm, in different organic solvents at concentration of 5×10^{-5} M, Table 4. Three absorption peaks were recorded in all spectra, Fig. 4. The shortest wavelength peak observed in the range of 250–270 nm may be attributed to a transition of the heterocyclic moiety of the molecule with $n \rightarrow \pi^*$ characteristic. The $n \rightarrow \pi^*$ assignment is confirmed by disappearing in acidic medium where the excitation of *n*-electrons is expected to be hindered by protonation. The second weak and shoulder-like peak located around 328–334 nm can be assigned to the $n \rightarrow \pi^*$ electronic transition of –N=N– group [25]. Finally, the λ_{max} peak must be related to a $\pi \rightarrow \pi^*$ transition contributing the whole π-electronic system of the compound in conjugation with the chromophore. There is no any correlation between the polarity and also donor-acceptor number of the used solvents with the main absorption wavelength. Due to the heteroatomic structure as well as the substantial strength of the intra and intermolecular hydrogen bondings, electron delocalization and solvent interactions are limited which is confirmed from the theoretical calculations.

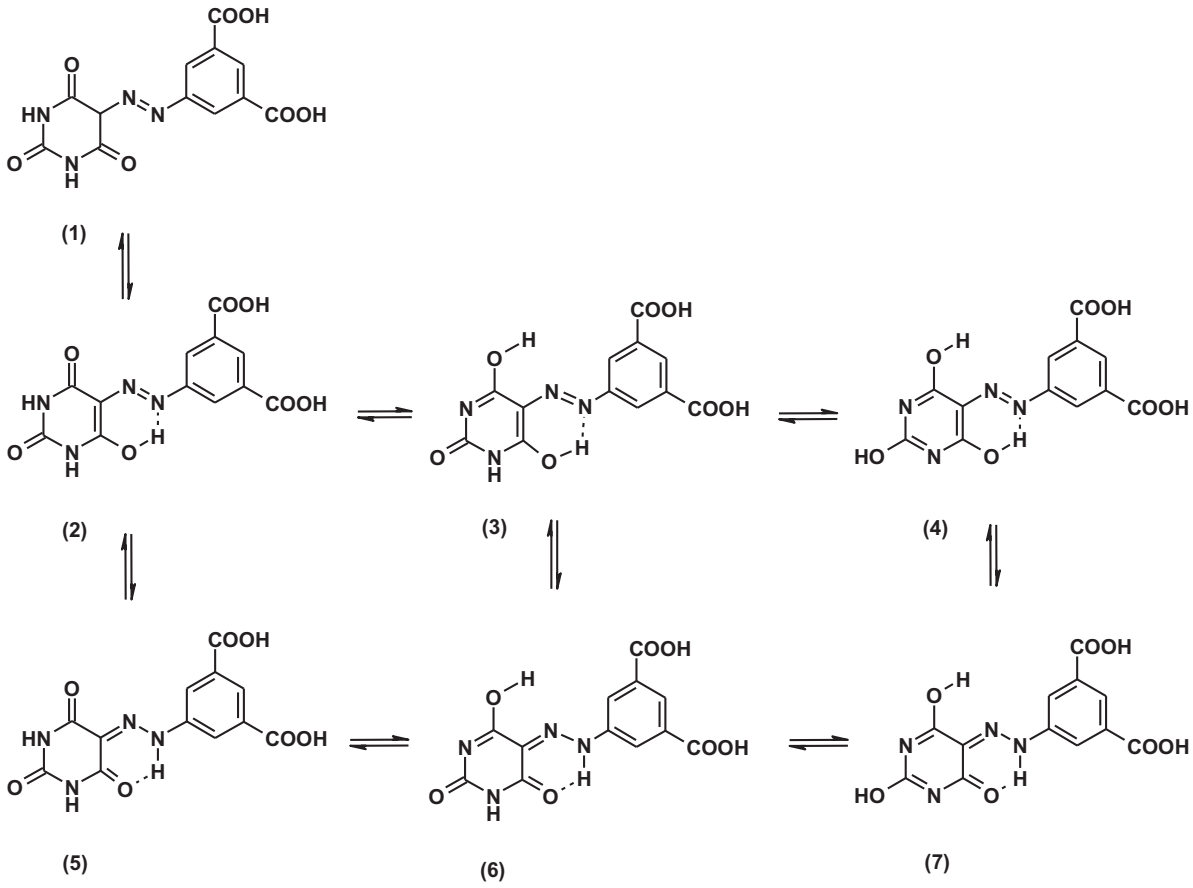

Scheme 2. Tautomeric structures of barbituric acid-based azo dye (**IV**).

Absorption spectrum of the azo dye was also recorded in aqueous media with different pHs, Fig. 5 and Table 5. The general pattern of the spectra in acidic media was similar to the spectra in organic solvents because the azo dye is as non-dissociated molecules. Of course, as mentioned above, protonation of the more basic site of the compound restricts the first absorption band around 256 nm. On the other hand, the second band appearing at 324 nm is disappeared with increasing pH. It seems completely dissociated molecules to be the preferred species in these conditions without absorption at the referred wavelength. The principle band displayed a blue shift in both alkaline and acidic solution relative to the neutral conditions. The plausible reason may be dissociation of the acidic functionalities and so weakening the electron accepting power of these electronegative segments of the molecule in alkaline solutions especially after pH 9. Whereas, the observed phenomenon in acidic solutions can arise from the protonation of the basic sites of the molecule which results to lower the HOMO energy level. Along with the increasing of hydronium concentration in the dye solution, azo dye molecules get more likely aggregated to form micellars [54]. The event was observed in our investigation as appearing flocculates and producing a colloidal solution with decreasing the pH to one. These results postulate that, the wavelength changes is believed to be a substituent effect than a tautomeric equilibration change between the azo and hydrazone configurations which might occur by changing pH.

The electron-poor heterocyclic pyrimidine and carboxy-functionalized benzene rings as the formative components of the azo chromophore strongly reduce the electron polarizibilty of the molecule. Thus the inter and intramolecular charge transfer between the components is diminished and the absorption maxima are significantly blue-shifted. In addition the cut-off wavelength of the azo dye in both aqueous and non aqueous solutions begins above 500 nm exhibiting good optical transparency.

The solid state spectrum (DRS) of the azo dye was also considered. It consisted of a band with a maximum around 317 nm which included a structureless red tail upto 448 nm. Since to stabilizing the hydrazone form with increasing intermolecular interactions, based on theoretical predictions, the red tail might show existence of associated forms of the dye molecule in that tautomeric form.

The FT IR spectrum of the compound could giving information of compact structure showed a high frequency peak assigned to an H-bonded proton and two imidic stretching peaks appeared at 3450, 3200 and 3079 cm^{-1} respectively. The other characteristic peaks comprised the stretching vibration bands of the carbonyl groups at 1720, 1670 and 1648 cm^{-1}(as a shoulder), two intense sharp bands at 1527 and 1397 cm^{-1} and a medium one at 1085 cm^{-1} assigned to the C═N, C—N and N—N stretching vibrations respectively, as well as two C—O stretching vibration bands at 1278 and 1218 cm^{-1}. According to these results and considering higher decomposition melting point and thermal stability of the azo dye, greater than 300 °C from TGA/DTA, the compound should be predominantly existed as a hydrazone-keto form (**5**) in the solid state [55].

In ^{1}H NMR spectrum of the azo dye, Fig. 6, a high deshielded peak attributable to a strongly intramolecular H-bonded proton was found at 14.05 ppm. Regarding the resonance of hydrazonic H-bonded OH protons appearing at a lower field, the predicted structure of the compound in solution polar media such as DMSO should be a tautomeric form containing intramolecular H-bonding like hydrazone-keto form (**5**). Furthermore, for N—H protons of pyrimidine-trione ring in barbituric segment, two peaks at 11.34 and 11.53 ppm are observed displaying their similar nature and an unsymmetrical structure for the molecule. The signal areas in the spectrum are in

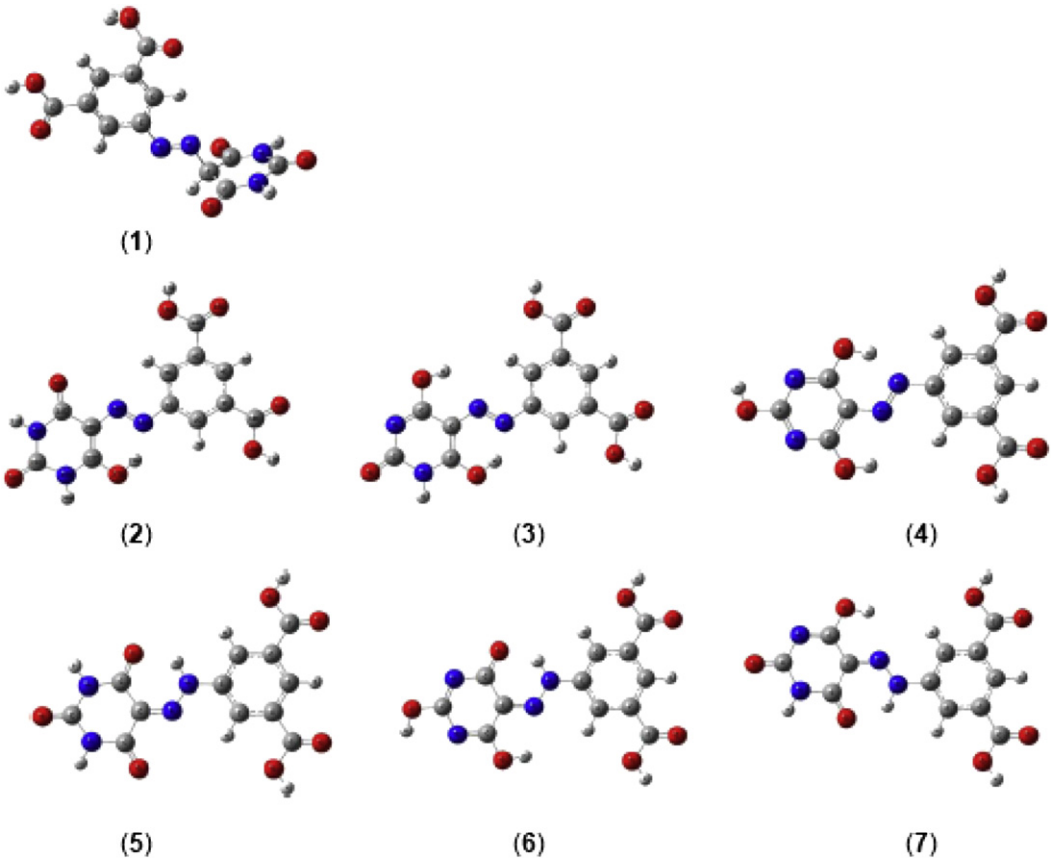

Fig. 1. Geometry-optimized structures of tautomeric forms of azo-dye (**IV**).

accord with the molecular structure prediction. It seems that excepting the H-bonded proton, the molecule lacks free phenolic protons, because possible exchanging of such protons with solvent could alter effectively the signal area ratios. It is previously well known that hydroxy pyrimidine can exist in the keto structure as barbituric acid [56]. Therefore, we suppose the structure (**5**), Scheme 2, to be the preferred form of the monomer in solution. The ^{13}C NMR spectrum, Fig. 7, also approves the above mentioned results.

Azo dyes having barbituric acid moieties display slight solubility in most organic solvents, high thermal stability and high melting point emanating from strong intermolecular hydrogen bondings. The solubility of azo dye (**IV**) was evaluated in different solvents. The results showed limited solubility in acidic or basic solvents such as acetic acid and pyridine, Table 6.

3.2. Model compound

A model reaction was conducted to evaluate the monomer reactivity and polymerization conditions using the azo dye and an aromatic amine, Scheme 3. The homogeneous reaction mixture

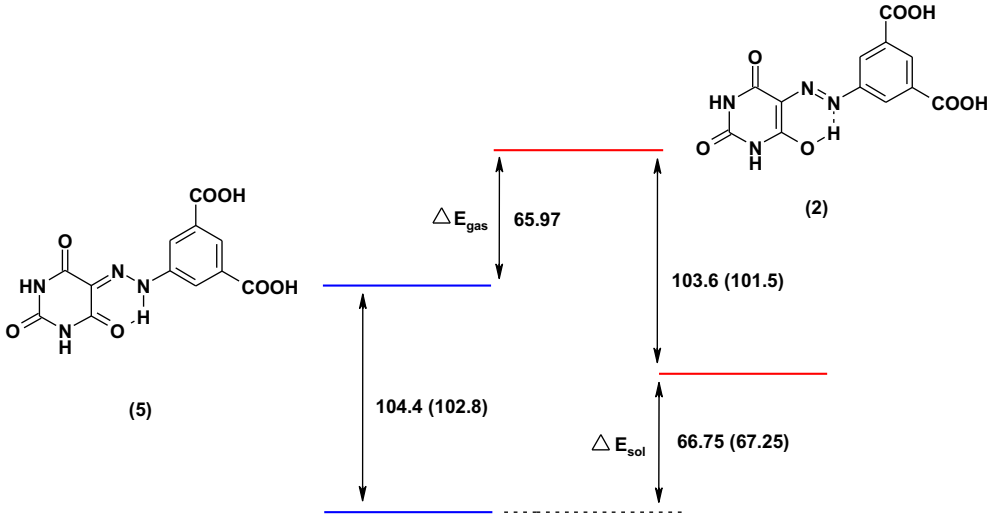

Fig. 2. Relative stability of azo (2) and hydrazone (5) tautomers predicted by DFT (B3LYP) calculations for gas phase and PCM for solution in terms of kJ/mol. The solvation stability values for DMSO are out of parentheses and for Methanol are inside.

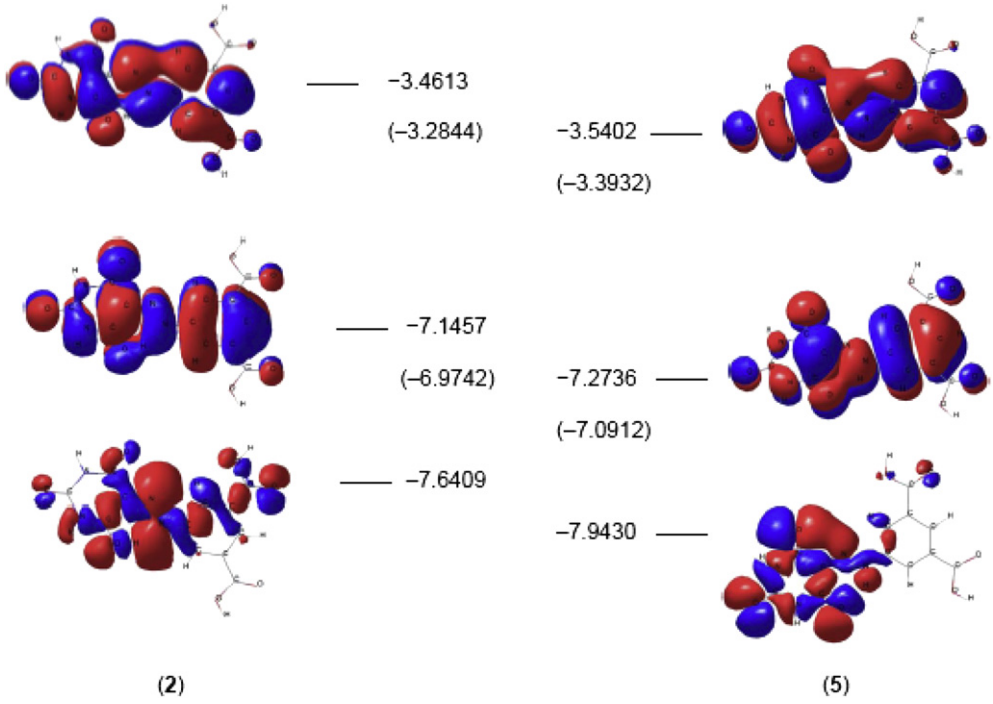

Fig. 3. Molecular orbital surface and energies of the main frontier molecular orbitals of azo (2) and hydrazone (5) tautomers (The out of parenthesis values are for gas phase and the inside ones are for solution).

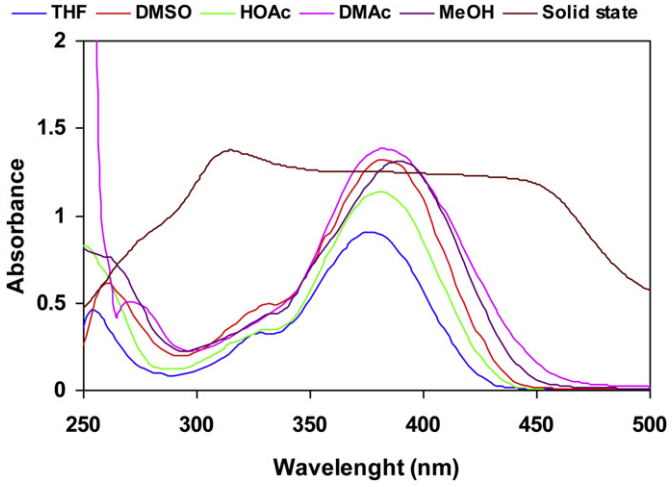

Fig. 4. Electronic absorption spectra of the azo dye in 5×10^{-5} M organic solutions and in solid state.

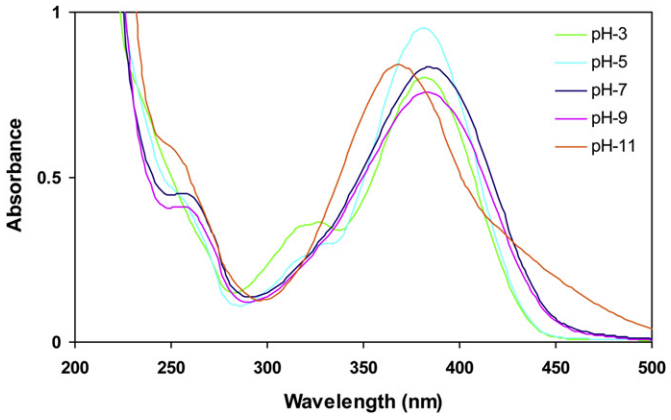

Fig. 5. Electronic absorption spectra of 10^{-5} M aqueous solutions of the azo dye with different pHs.

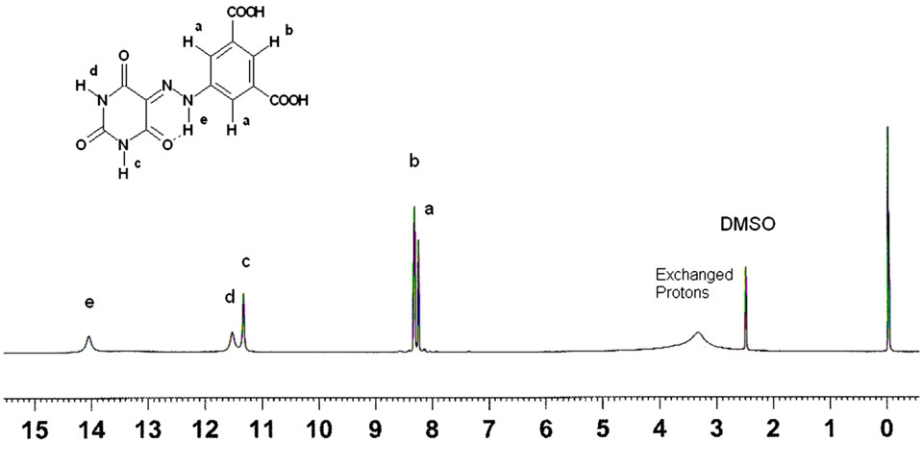

Fig. 6. ^{1}H NMR spectrum (300 MHz, DMSO-d_6) of azo dye (**IV**).

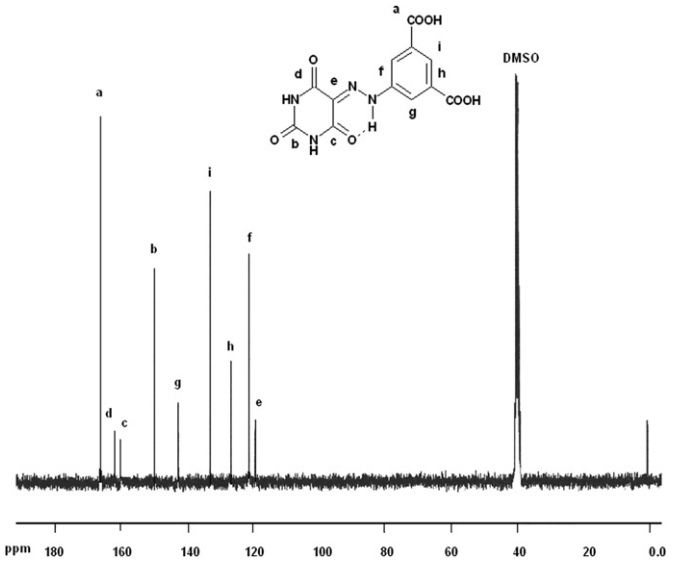

Fig. 7. ^{13}C NMR (75 MHz, DMSO-d_6) spectrum of azo dye (**IV**).

produced compound (**VI**) which was not soluble in 5 and 10% $NaHCO_3$ and NaOH aqueous solutions.

The chemical structure and purity of the reaction product were confirmed by FT IR, ^1H NMR and ^{13}C NMR spectroscopic techniques together with thin layer chromatography (TLC). The characteristic peaks of the FT IR spectrum appeared at 3425 cm^{-1} (stretching vibration of the amide NH), 1741, 1722 and 1665 cm^{-1} (C=O of the barbituric acid ring) as well as 1597 cm^{-1} (−C=N−), 1650 cm^{-1} (amide C=O) and 1395 cm^{-1} (−C−N−) were indications of the azo−triketo form in the solid state.

^1H and ^{13}C NMR spectra of the model compound showed the same features as the monomer spectra, Figs. 8 and 9: a distinct hydrazonic peak at 14.23 ppm and two different N−Hs peak's of barbituric ring which have been appeared at 10.88 and 11.39 ppm in ^1H NMR spectrum. The other signals are simply attributed to the compound. Here again, the prominence of the hydrazone-keto form in tautomeric equilibrium in solution is evidenced.

3.3. Azo-barbituric polyamides (PA***a-h***)

3.3.1. Synthetic inspection

A series of aromatic polyamides with pendant azo−barbituric groups were synthesized by the Yamazaki−Higashi phosphorylation

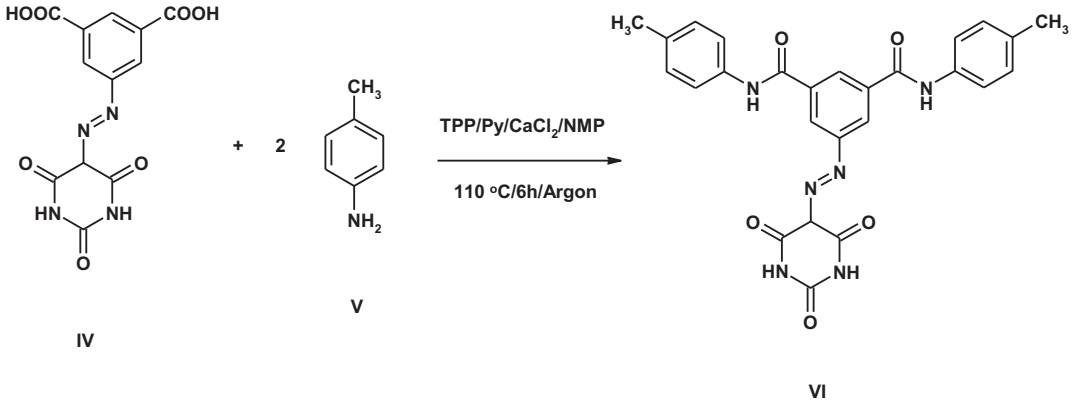

Scheme 3. The synthetic route of the model compound.

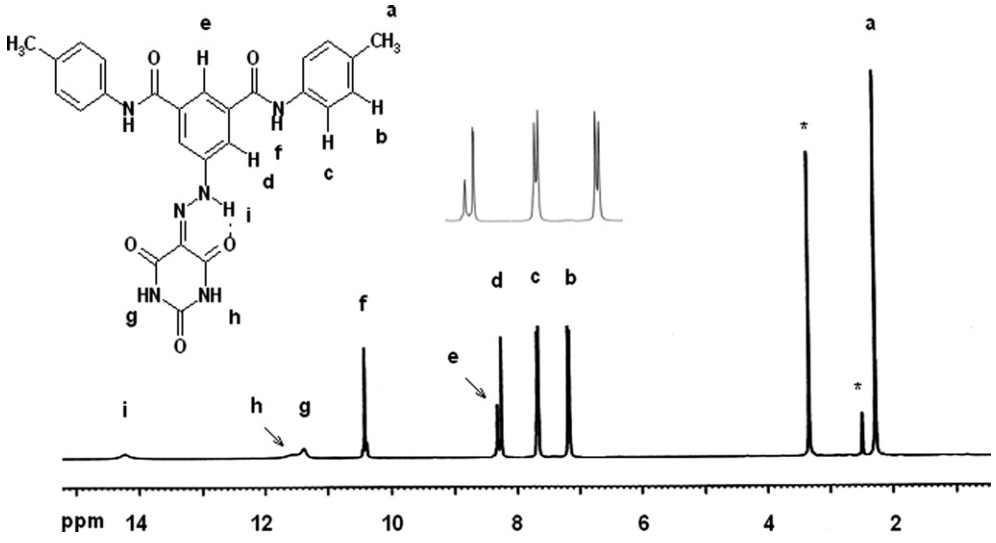

Fig. 8. ^1H NMR spectrum (300 MHz, DMSO-d_6) of the model compound. The asterisked peaks relate to the solvent.

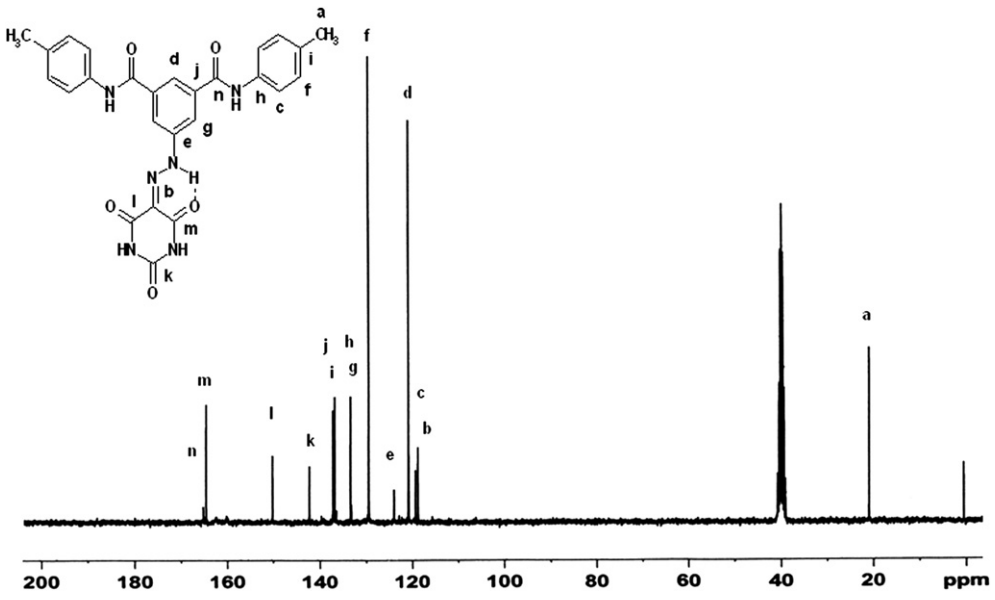

Fig. 9. ^{13}C NMR spectrum (75 MHz, DMSO-d_6) of the model compound.

reaction from different aromatic diamines (**VIIa**–**h**) and azo dye (**IV**), Scheme 4. The reaction parameters such as reaction time, temperature, solvent and monomer concentration were optimized. Surprisingly, higher yield and polymer viscosity were obtained in DMAc than NMP. The reaction mixture was heterogeneous in the latter solvent. Fig. 10 represents the results of temperature and reaction time dependence of polymerization yield and product viscosities. The curves simply show the trends observed in polycondensation reactions.

All polymerizations proceeded as homogeneous and transparent solutions throughout the reaction. The final viscous mixtures were poured into the methanol to produce the polyamides with the yields in the range of 90–96%. The results of some measurements on PAs are summarized in Table 7.

The polymer formation was confirmed by infrared spectroscopy and chemical solubility tests in 5% aqueous solutions of $NaHCO_3$ and NaOH. A typical FT-IR spectrum of the polyamides is shown in Fig. 11. The presence of the characteristic peaks of the amide groups

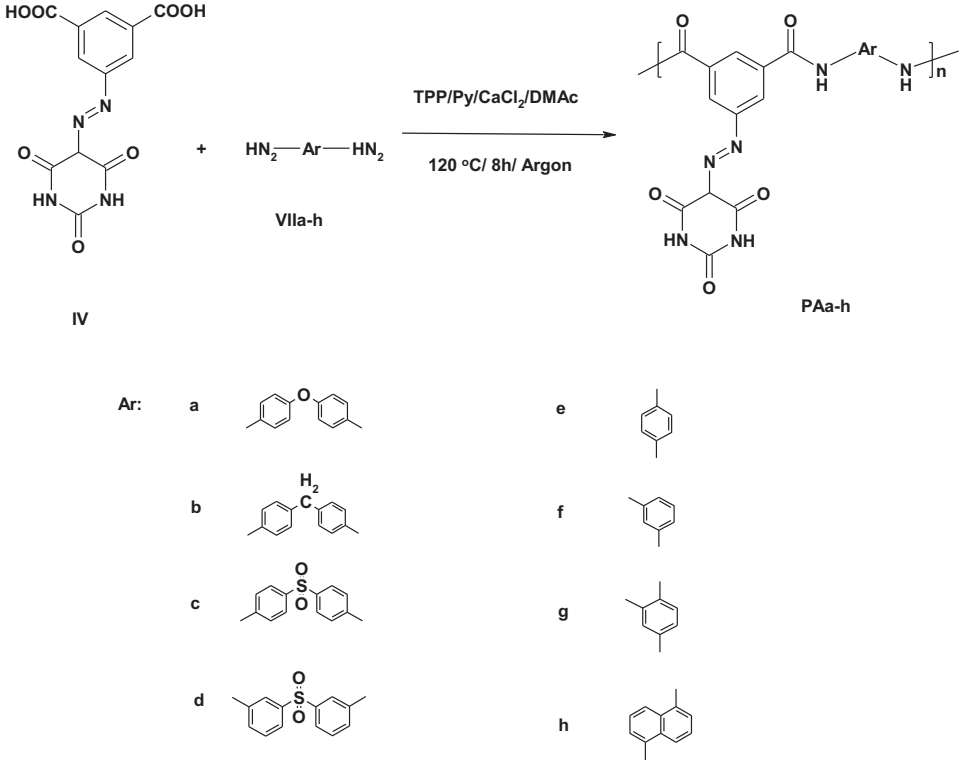

Scheme 4. The synthetic route of the azo-polyamides.

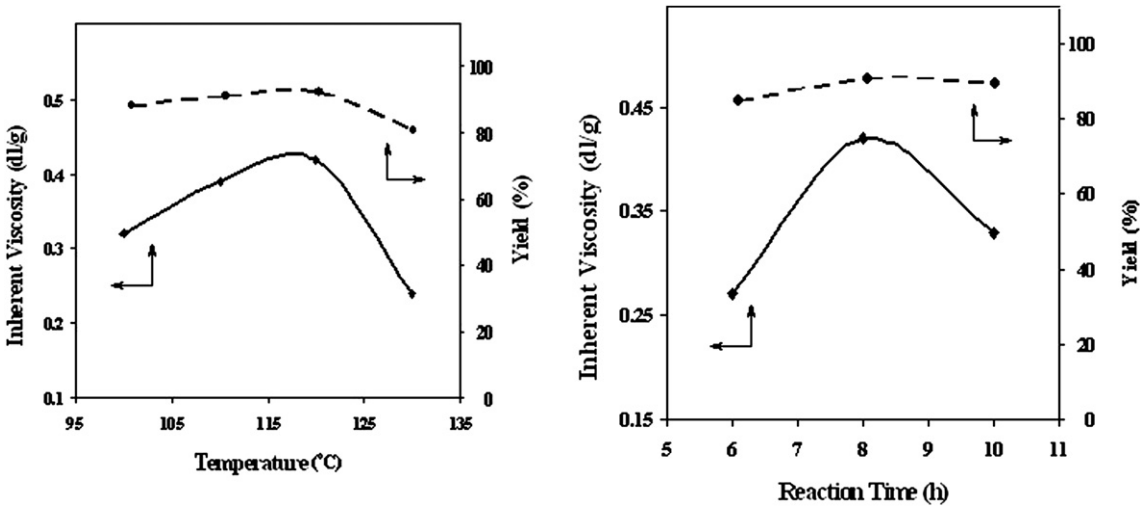

Fig. 10. Temperature and reaction time dependence of polymerization yield and product viscosities.

and the absence of the original peaks arising from the carboxylic functions in the corresponding diacid (**IV**) confirm the polymer synthesis.

3.3.2. Polymer properties

The solubility of PA**a**–**h** was tested in various organic solvents at the concentration of 0.05 g/dl, Table 8. Polyamides PA**a**–**d** showed excellent solubility in aprotic polar solvents such as NMP, DMSO, DMF and DMAC at room temperature. The enhanced solubility of these polyamides is believed to be related to the presence of flexible linkages in the polymer backbone. The solubility process of the polyamides was very slow because of the presence of the polar protic barbituric groups. The lower mobility of the solvent in polymer matrix could also influence their film forming ability.

The azo-polyamide films were prepared from their 8% solutions in NMP, DMAc and DMF by casting onto glass plates based on drop coating method. The layered solutions dried in a low humidity air environment at ambient temperature for two weeks. Some of the resulting films from DMAC or DMF solution (PA**a,b,c,d,f**) were opaque, whereas their NMP solutions and the others produced transparent layers. Seemingly, aggregation of polymer chains were occurred in the former solvents whereas the more polar one, NMP, suppressed the proposed phenomenon and offered a better film formability. The resulting films exhibited various degrees of shattering, as presented in Table 7. High boiling point and low diffusion rate of the used solvents having efficient interactions with the polymer matrix are determinant factors in the film forming process.

DMAc solutions of the synthesized polymers were exposed to UV–vis spectroscopy to monitor the absorption characteristics compared with the monomer as a molecular azo-dye. As Fig. 12 implies, the main chromophore absorption of the polymers remained virtually unaltered, whereas the lower band related to barbituric segment appeared at higher wavelengths than to the monomer. The azo chromophore is located inside the molecule, far from effective solvent interactions both in polymeric and molecular structure, whereas barbituric unit can be better accessible to solvent molecules in a molecular form than a polymeric one. Probably the excited state of $n \rightarrow \pi^*$ transition of barbituric unit is unstablized with increasing solvation by a polar aprotic solvent.

Table 7
Some of the properties of the synthesized polyamides (PA**a**–**h**).

Polymer code	Yield (%)	η_{inh} (dl/g) [a]	T_D (°C) [b]	Film[c]	Characteristic IR absorptions (cm^{-1})
PA**a**	96.8	0.29	>350	Shattered to brittle large pieces	3285 (m), 3058 (w), 2924 (m), 1734 (s), 1670 (s), 1602 (s), 1499 (s), 1466 (s), 1235 (s), 1170 (s)
PA**b**	93.6	0.42	>350	Shattered to brittle large pieces	3315 (m), 3059 (w), 2830 (m), 1734 (s), 1702 (s), 1669 (s), 1598 (s), 1514 (s), 1466 (s), 1320 (s), 1256 (s), 1127 (m)
PA**c**	96.7	0.20	>350	Shattered to brittle large pieces	3252 (m), 3096 (w), 2853 (m), 1734 (s), 1672 (s), 1590 (s), 1522 (s), 1466 (m), 1420 (m), 1400 (s), 1319 (s), 1251 (m), 1185 (m)
PA**d**	95.7	0.18	>350	Shattered to brittle large pieces	3250 (m), 3076 (w), 2825 (m), 1734 (s), 1673 (s), 1595 (s), 1525 (s), 1479 (s), 1421 (m), 1302 (m), 1254 (m), 1150 (s), 1100 (m)
PA**e**	90.9	0.44	>350	Shattered to brittle small pieces	3216 (m), 3060 (w), 2851 (m), 1734 (s), 1670 (s), 1560 (w), 1515 (s), 1458 (w), 1404 (w), 1314 (s), 1248 (m), 1131 (s)
PA**f**	90.0	0.24	>350	Shattered to brittle small pieces	3251 (m), 3056 (w), 2818 (m), 1733 (s), 1702 (s), 1664 (s), 1609 (s), 1542 (s), 1483 (m), 1417 (m), 1350 (w), 1249 (s)
PA**g**	90.5	0.38	>350	Shattered to brittle large pieces	3198 (m), 3062 (w), 2819 (m), 1734 (s), 1670 (w), 1599 (s), 1522 (s), 1412 (m), 1340 (w), 1248 (s), 1136 (w)
PA**h**	95.0	0.31	>350	Shattered to brittle small pieces	3224 (m), 3068 (w), 2850 (m), 1734 (s), 1670 (s), 1601 (m), 1523 (s), 1458 (w), 1413 (m), 1338 (s), 1267 (s), 1132 (w)

[a] Measured at a concentration of 0.5 g/dl in H_2SO_4 (98%) at 30 °C.
[b] Onset decomposition temperature measured by melting point apparatus.
[c] Solution (8% w/v in NMP, DMAc and DMF) casting film via drop coating technique, ability and quality of films.

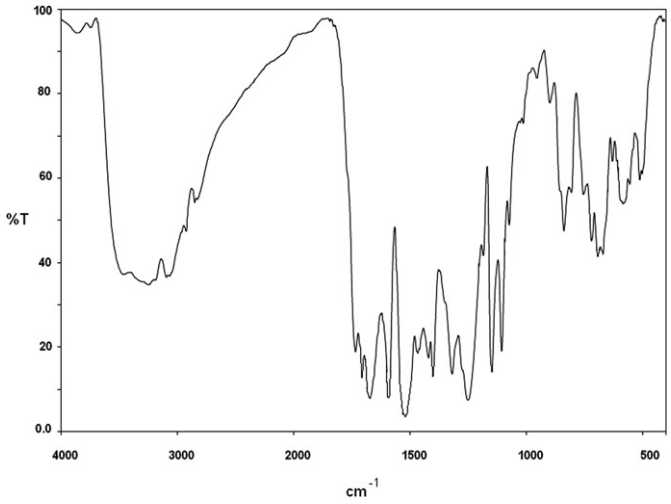

Fig. 11. FT IR spectrum of the polyamide PA**c** in KBr.

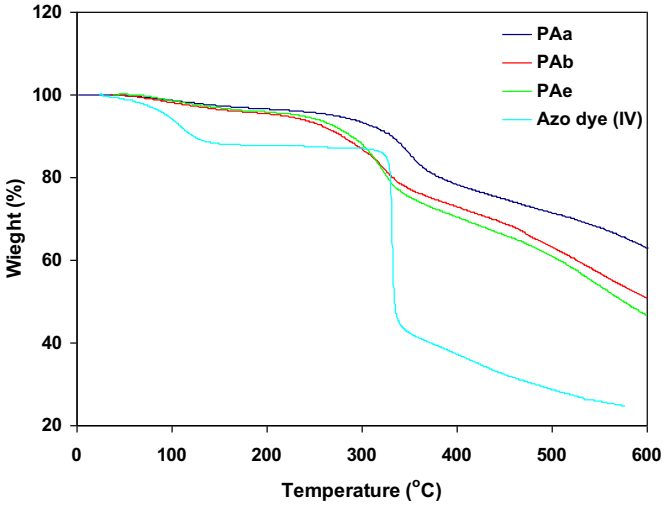

Fig. 13. TGA thermograms of polyamides PA**a**, PA**b**, PA**e** and azo dye (**IV**).

Table 8
The solubility behavior of the polyamides (PA**a**–**h**).[a]

Solvents	PA**a**	PA**b**	PA**c**	PA**d**	PA**e**	PA**f**	PA**g**	PAh
NaOH (aq 5%)	−(−)	−(−)	−(−)	−(−)	−(−)	−(−)	−(−)	−(−)
MeOH	−(−)	−(−)	−(−)	−(−)	−(−)	−(−)	−(−)	−(−)
HOAc	−(−)	−(−)	−(−)	−(−)	−(−)	−(−)	−(−)	−(−)
THF	−(−)	−(−)	−(−)	−(−)	−(−)	−(−)	−(−)	−(−)
DMAc	+(+)	+(+)	+(+)	+(+)	±(+)	±(±)	+(+)	+(+)
DMF	+(+)	+(+)	+(+)	+(+)	±(±)	±(±)	+(+)	±(±)
NMP	+(+)	+(+)	+(+)	+(+)	+(+)	+(+)	+(+)	+(+)
DMSO	+(+)	+(+)	+(+)	+(+)	+(+)	+(+)	+(+)	+(+)
H_2SO_4	+(+)	+(+)	+(+)	+(+)	+(+)	+(+)	+(+)	+(+)

[a] Solubility concentration: 5 mg/ml; ±, partially soluble; −, insoluble; +, soluble; symbol out of parenthesis is at room temperature; symbol into the parenthesis is on heating at 70 °C; DMAc, N,N-dimethylacetamide; DMF, N,N-dimethylformamide; DMSO, dimethylsulfoxide; NMP, N-methyl-2-pyrrolidone; THF, tetrahydrofuran.

The thermal stability of the azo-PAs was investigated by TGA analysis at a heating rate of 10 °C/min under a nitrogen atmosphere and compared with the monomer thermogram. Typical thermal traces of PA**a**,**b**,**e** are shown in Fig. 13. The polymers were stable up to 250 °C and their main decomposition process including azo degradation was initiated above 280 °C. Furthermore, the TGA profiles represented high carbonized residue and limiting oxygen index at 600 °C, indicating good fire retardant property of the azo-polymers. Differential scanning calorimetry (DSC) of the selected polymers (PA**a**,**b**,**e**), Fig. 14, showed high glass transition temperatures. Numerous H-bonding between side barbituric groups weaken the thermal effects on segmental motions of the polymer chains. Numerical data related to the thermal properties of polyamides PA**a**, PA**b** and PA**e** were depicted in Table 9. In DSC curves, no other thermal changes, except glass transition were observed

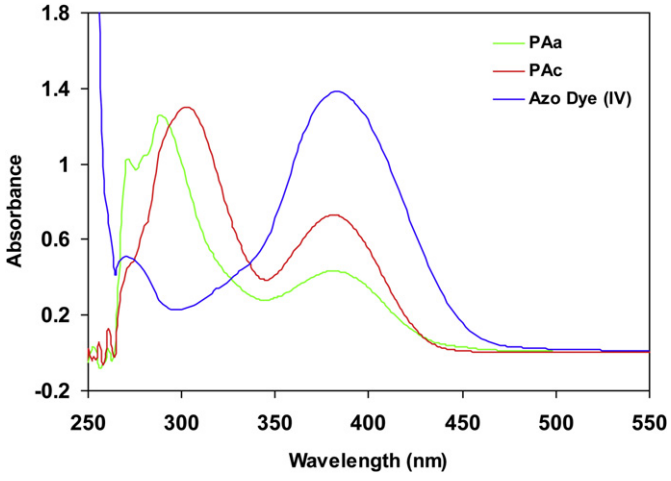

Fig. 12. Electronic absorption spectra of 10^{-5} g/ml solution of azo-dye (**IV**), PA**a** and PA**c** in DMAc.

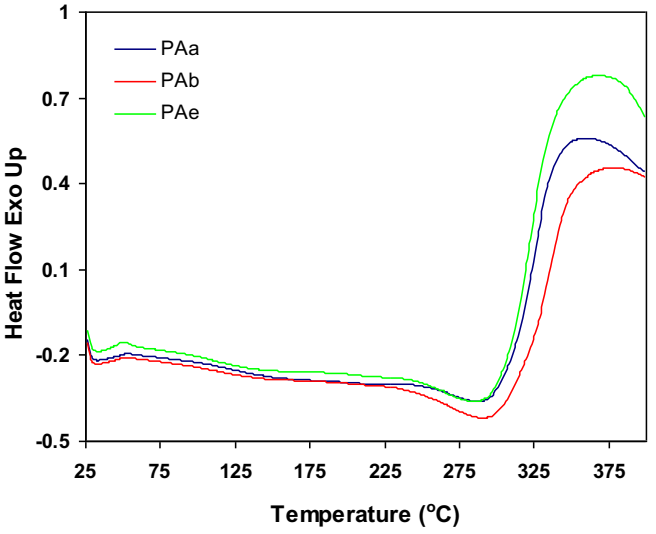

Fig. 14. DSC Traces of polyamidse PA**a**, PA**b** and PA**e**.

Table 9
Thermal properties data of polyamides PA**b**, PA**c** and PA**d**.

Polymer code	T_d (°C)[a]	T_{max} (°C)[b]	T_g (°C)	Char yield (%)[c]	LOI[d]
PA**a**	320	360	270	58.8	41.0
PA**b**	280	320	260	51.3	38.0
PA**e**	285	325	262	47.2	36.4

[a] Onset of decomposition temperature.
[b] Maximum rate of decomposition temperature.
[c] Carbonized residue at 600 °C.
[d] Limiting oxygen index, LOI = 17.5 + 0.4CY, CY = Char Yield.

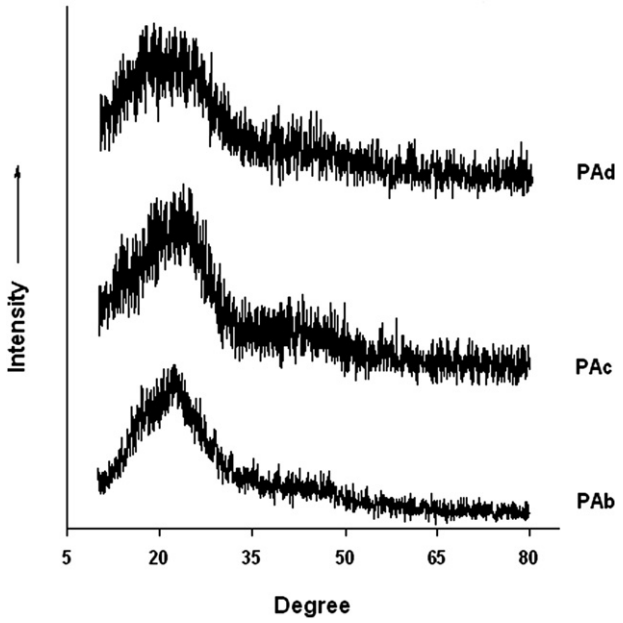

Fig. 15. Wide-angle X-ray diffractograms of polyamides PA**b**, PA**c** and PA**d**.

below decomposition temperature, indicating the amorphous nature of the polymers. This morphology was confirmed by XRD patterns for some of the synthesized polymers showed a broad peak in the range of 10–80 2Θ illustrating a weak ordered structure, Fig. 15.

4. Conclusions

A novel barbituric acid-based dicarboxilic acid monomer containing an azo chromophore was synthesized and fully characterized by spectroscopic techniques. The results resolved that the compound could exist as an azo-triketo form in both solid state and solution. DFT quantum-chemical calculations in gas phase and solution showed the preference of the hydrazone-keto form between seven possible tautomeric structures. Patterns of charge density distribution of HOMO–LUMO in the favored form revealed no substantial charge perturbation occurring in electron excitation. It confirmed the empirical results related to partial solvent effects on photo-absorption behavior. A model reaction was utilized to approve that the imidic protons of barbituric segment of the monomer do not interfere in the amid formation reaction. Thereafter, polycondensation of the azo-diacid with several aromatic diamines resulted to a series of side chain azo-polyamides. The polymers showed good solubility only in polar aprotic solvents and were not soluble in basic or acidic aqueous solutions. Solution casting of the synthesized polyamides gave clear, shattered and brittle films. The resulting azo-PAs exhibited UV–vis absorption behavior comparable to the monomer and thermal stability in thremogravimetric analysis with temperature of 5% weight loss upper than 240 °C and glass transition temperatures in the range of 260–264 °C.

Acknowledgement

The Graduate Council of University of Mohaghegh Ardabili, Iran, is gratefully acknowledged for their financial support.

References

[1] Zollinger H. Color chemistry. 3th ed. Switzerland: Verlag Helvetica Chimica Acta; 2003.
[2] Moylan CR, McNelis BJ, Nathan LC, Marques MA, Hermstad EL, Brichler BA. Challenging the auxiliary donor effect on molecular hyperpolarizability in thiophene-containing nonlinear chromophores: X-ray crystallographic and optical measurements on two new isomeric chromophores. J Org Chem 2004; 69:8239–43.
[3] Raposo MMM, Sousa AMRC, Fonseca AMC, Kirsch G. Thienylpyrrole azo dyes: synthesis, solvatochromic and electrochemical properties. Tetrahedron 2005; 61:8249–56.
[4] Abd-El-Aziz AS, Shipman PO, Shipley PR, Boden BN, Aly S, Harvey PD. Homo- and Co-polymers of norbornene containing aryl- and hetaryl-azo dyes; synthesis and sensing properties. Macromol Chem Phys 2010;210:2099–106.
[5] Karci F. Synthesis of disazo dyes derived from heterocyclic components. Color Technol 2005;121:275–80.
[6] He M, Zhou Y, Liu R, Dia J, Cui Y, Zhang T. Novel nonlinearity–transparency thermal stability trade-off of thiazolylazopyrimidine chromophores for nonlinear optical application. Dyes Pigments 2009;80:6–10.
[7] Masoud MS, Ali AE, Shaker MA, Ghani MA. Solvatochromic behavior of the electronic absorption spectra of some azo derivatives of amino pyridines. Spectrochim Acta A Mol Biomol Spectrosc 2004;60:3155–9.
[8] Batista RMF, Costa SPG, Belsley M, Raposo MMM. Synthesis and second-order nonlinear optical properties of new chromophores containing benzimidazole, thiophene, and pyrrole heterocycles. Tetrahedron 2007;63:9842–9.
[9] Raposo MMM, Ferreira AMFP, Amaro M, Belsley M, Moura JCVP. The synthesis and characterization of heterocyclic azo dyes derived from 5-N, N-dialkylamino-2,2'-bithiophene couplers. Dyes Pigments 2009;83:59–65.
[10] Zhong AM, Zhou YM, Qiu FX. Synthesis and characterization of thiazole chromophores with high second-order polarizability. Acta Chim Sinica 2006; 64:343–7.
[11] Konstantinov T, Petrov P. On the synthesis of some bifunctional reactive triazine dyes. Dyes Pigments 2002;52(2):115–20.
[12] Coelho PJ, Carvalho LM, Moura JCVP, Raposo MMM. Novel photochromic 2,2′-bithiophene azo dyes. Dyes Pigments 2009;82:130–3.
[13] Sujamol MS, Athira CJ, Sindhu Y, Mohanan K. Synthesis, spectroscopic characterization, electrochemical behaviour and thermal decomposition studies of some transition metal complexes with an azo derivative. Spectrochim Acta A Mol Biomol Spectrosc 2010;75:106–12.
[14] Chen LJ, Cui YJ, Qian GD, Wang MQ. Synthesis and spectroscopic characterization of an alkoxysilane dye containing azo-benzothiazole chromophore for nonlinear optical applications. Dyes Pigments 2007;73:338–43.
[15] Batista RMF, Costa SPG, Malheiro EL, Belsley M, Raposo MMM. Synthesis and characterization of new thienylpyrrolylbenzothiazoles as efficient and thermally stable nonlinear optical chromophores. Tetrahedron 2007;63:4258–65.
[16] Pan QW, Zhang ZY, Fang CS, Wei S, Gu QT, Wu XW. Synthesis and characterization of thiazolylazo chromophore for nonlinear optical applications. Mater Lett 2001;50:284–6.
[17] Qiu L, Shen YQ, Hao JM, Zhai JF, Zu FH, Zhang T. Study on novel second-order NLO azo-based chromophores containing strong electron-withdrawing groups and different conjugated bridges. J Mater Sci 2004;39:2335–40.
[18] Dirk CW, Katz HE, Schilling ML. Use of thiazole rings to enhance molecular second-order nonlinear optical susceptibilities. Chem Mater 1990;2:700–5.
[19] Hrobarik P, Sigmundova I, Zahradnık P. Preparation of novel push–pull benzothiazole derivatives with reverse polarity: compounds with potential nonlinear optic application. Synthesis 2005;4:600–4.
[20] Lorenz M, Schuendehuette KH. Derivatives of azobarbituric acid or salts or complexes thereof. US4,628,082; 1986.
[21] Levina RY, Velichko FK. Advances in the chemistry of barbituric acids. Russ Chem 1960;29:437–59.
[22] Karci F, Karci F. The synthesis and solvatochromic properties of some novel heterocyclic disazo dyes derived from barbituric acid. Dyes Pigments 2008;77: 451–6.
[23] Ucun F, Saglam A, Kara I, Karci F. Investigation of ground state tautomeric form of a heterocyclic disazo dye derived from barbituric acid by ab initio Hartree-Fock and density functional theory calculations. J Mol Struct Theochem 2008;868:94–100.
[24] Amrallah AH, Abdalla NA, El-Haty EY. Spectrophotometric studies on some Arylazo barbituric acids and Arylazo pyrimidine in organic solvents and in buffer solutions. J Chin Chem Soc 2007;54:1629–37.
[25] Gup R, Giziroglu E, Kirkan B. Synthesis and spectroscopic properties of new azo-dyes and azo-metal complexes derived from barbituric acid and aminoquinoline. Dyes Pigments 2007;73:40–6.
[26] Barrett CJ, Mamiya J, Yager KG, Ikeda T. Photo-mechanical effects in azobenzene-containing soft materials. Soft Matter 2007;3:1249–61.
[27] Yager KG, Barrett CJ. Novel photo-switching using azobenzene functional materials. J Photoch Photobio A 2006;182:250–61.
[28] Kasture PP, Sonawane YA, Rajule RN, Shankarling GS. Synthesis and characterisation of benzothiazole-based solid-state fluorescent azo dyes. Color Technol 2010;126:248–52.
[29] Tsai CC, Chao TY, Lin HL, Liu YH, Chang HL, Liu YL, et al. The facile synthesis and optical nonlinearity of hyperbranched polyaspartimides with azobenzene dyes. Dyes Pigments 2009;82:31–9.

[30] Li N, Lu J, Xia X, Xu Q, Wang L. Synthesis of third-order nonlinear optical polyacrylates containing an azobenzene side chain via atom transfer radical polymerization. Dyes Pigments 2009;80:73–9.
[31] Xin Z, Sanda F, Endo T. Synthesis and characterization of colored monomers based on 2-methylresorcinol. Dyes Pigments 2001;49:1–7.
[32] Al-M Nayef S. Synthesis and characterization of new unsaturated polyesters and copolyesters containing azo groups in the main chain. Eur Polym J 2003; 39:1025–33.
[33] Bojinov V, konstantinova T. Synthesis of polymerizable 1,8-naphthalimide dyes containing hindered amine fragment. Dyes Pigments 2002;54:239–45.
[34] Zhu ZH, Li Q, Zeng Q, Zh Li, Zh Li, Qin J, et al. New azobenzene-containing polyurethanes: post-functional strategy and second-order nonlinear optical properties. Dyes Pigments 2008;78:199–206.
[35] Luo J, Qin J, Kang H, Ye C. Synthesis and characterization of accordion main-chain azo-dye polymers for second-order optical non-linearity. Polym Int 2000;49:1302–7.
[36] Yu X, C. Xinog, You Y, Dong L, Yao J. Aromatic azo-polyamide electrolyte with liquid crystal structure and photoelectrical properties. Synth Met 2008;158:375–8.
[37] Sieung Ju K, Beom Jun K, Dong Wook G, Se Hun K, Soo Young P, Ju Hyun L, et al. Photoactive polyamideimides synthesized by the polycondensation of azo-dye diamines and rosin derivative. J Appl Polym Sci 2001;79:687–95.
[38] Hamciuc E, Sava I, Bruma M, Kopnick T, Schulz B, Sapich B, et al. New poly(amide-imide)s containing cinnamoyl and azobenzene group. Polym Advan Technol 2006;17:641–6.
[39] Faghihi Kh, Hagibeygi M. New polyamides containing azobenzene unites and hydantoin derivatives in ahain: synthesis and characterization. J Eur Polym 2003;39:2307–14.
[40] Gubbelmans E, Verbiest T, Van Beylen M, Persoons A, Samyn C. Chromophore-functionalized polyamides with high-poling stabilities of the nonlinear optical effect at elevated temperature. Polymer 2002;43:1581–5.
[41] Becke AD. Density functional thermochemistry. III. The role of exact exchange. J Chem Phys 1993;98:5648–52.
[42] Schaefer A, Horn H, Ahlrichs R. Fully optimized contracted Gaussian basis sets for atoms Li to Kr. J Chem Phys 1992;97:2571–7.
[43] Schaefer A, Huber C, Ahlrichs R. Fully optimized contracted Gaussian basis sets of triple zeta valence quality for atoms Li to Kr. J Chem Phys 1994;100: 5829–35.
[44] Granovsky AA. Firefly version 7.1.G, www http://classic.chem.msu.su/gran/firefly/index.html.
[45] Schmidt MW, Baldridge KK, Boatz JA, Elbert ST, Gordon MS, Jensen JH, et al. General atomic and molecular electronic structure system. J Comput Chem 1993;14:1347–63.
[46] Tomasi J, Mennucci B, Cammi R. Quantum mechanical continuum salvation models. Chem Rev 2005;105:2999–3094.
[47] Pavlovic G, Racane L, Cicak H, Kulenovic VT. The synthesis and structural study of two benzothiazolyl azo dyes: X-ray crystallographic and computational study of azo–hydrazone tautomerism. Dyes Pigments 2009;83:354–62.
[48] Ebead YH. Spectrophotometric investigations and computational calculations of prototropic tautomerism and acid–base properties of some new azo dyes. Dyes Pigments 2011;92:705–13.
[49] Oziminski WP, Dobrowolski JC, Mazureka AP. DFT studies on tautomerism of C5-substituted 1,2,4-triazoles. J Mol Struct Theochem 2004;680:107–15.
[50] Yasuyo O, Toshio H, Mie H, Zenzo M. Substituent effects on the photofading of disperse azo dyes on poly(ethylene terephthalate) substrate. Color Technol 2010;126:127–39.
[51] Tripathi S, Vasudev I, Ray A. Photofading of azo dyes: a theoretical study. Color Technol 2008;124:151–8.
[52] Kim SD, Park EJ. Relation between chemical structure of yellow disperse dyes and their lightfastness. Fiber Polym 2001;2:159–63.
[53] Willy H, Klaus H, Wilker G, Obleier H, Winter R. Industrial organic pigment, production, properties application. 3th ed. Weinheim: Wiley-VCH; 2004.
[54] Wang L, Pan X, Wang F, Yang L, Liu L. Structure–properties relationships investigation on the azo dyes derived from benzene sulfonamide intermediates. Dyes Pigments 2008;76:636–45.
[55] Gordon PF, Gregory P. Organic chemistry in colour. Berlin: Springer-Verlag; 1983. p. 96–108.
[56] Bandekar J, Zundel G. The role of C=O transition dipole–dipole coupling interaction in uracil. Spectrochim Acta 1983;39A:337–41.